# DANISH METEOROLOGICAL INSTITUTE

## —— SCIENTIFIC REPORT ——

## 01-05

# Diagnostic and Prognostic Equations for the Depth of the Stably Stratified Ekman Boundary Layer

**Sergej Zilitinkevich, Alexander Baklanov,
Jutta Roost, Ann-Sofi Smedman,
Vasiliy Lykosov and Pierliugi Calanca**

**COPENHAGEN 2001**

# DIAGNOSTIC AND PROGNOSTIC EQUATIONS FOR THE DEPTH OF THE STABLY STRATIFIED EKMAN BOUNDARY LAYER

Sergej Zilitinkevich[1], Alexander Baklanov[2], Jutta Rost[1,3], Ann-Sofi Smedman[1], Vasiliy Lykosov[1,4] and Pierliugi Calanca[5]

[1] Department of Earth Sciences, Meteorology, Uppsala University, SE-752 36 Uppsala, Sweden
[2] Danish Meteorological Institute, DK-2100, Copenhagen, Denmark
[3] Meteorological Institute, University of Freiburg, D-79085 Freiburg, Germany
[4] Institute of Numerical Mathematics, Russian Acad. Sci., 117333 Moscow, Russia
[5] Swiss Federal Research Station for Agroecology and Agriculture, FAL/IUL, CH-3003 Bern, Switzerland

# DIAGNOSTIC AND PROGNOSTIC EQUATIONS FOR THE DEPTH OF THE STABLY STRATIFIED EKMAN BOUNDARY LAYER

Sergej Zilitinkevich[1], Alexander Baklanov[2], Jutta Rost[1,3], Ann-Sofi Smedman[1], Vasiliy Lykosov[1,4] and Pierliugi Calanca[5]

[1] Department of Earth Sciences, Meteorology, Uppsala University, SE-752 36 Uppsala, Sweden
[2] Danish Meteorological Institute, DK-2100, Copenhagen, Denmark
[3] Meteorological Institute, University of Freiburg, D-79085 Freiburg, Germany
[4] Institute for Numerical Mathematics, Russian Acad. Sci., 117333 Moscow, Russia
[5] Swiss Federal Research Station for Agroecology and Agriculture, FAL/IUL, CH-3003 Bern, Switzerland

## Abstract

Refined diagnostic and prognostic equations for the depth of the stably stratified barotropic Ekman boundary later (SBL) are derived employing a recently developed non-local formulation for the eddy viscosity. In well studied cases of the thoroughly neutral SBL, the nocturnal atmospheric SBL and the oceanic SBL dominantly affected by the static stability in the thermocline, the proposed diagnostic equation reduces to the Rossby-Montgomery, Zilitinkevich and Pollard-Rhines-Thompson equations, respectively. In its general form it is applicable to a range of regimes including long-lived atmospheric SBLs affected by the near-surface buoyancy flux and the static stability in the free atmosphere. Both diagnostic and prognostic SBL depth equations are validated against recent data from atmospheric measurements.

Keywords: boundary-layer depth, stable stratification, Ekman layer.

## 1. Introduction

The depth of geophysical (atmospheric and oceanic) turbulent boundary layers, $h$, is needed in a number of practically important problems such as pollution dispersion, wind engineering, air-sea interaction, weather prediction and climate modelling. The nature of these layers is critically dependent on the type of static stability: stable or unstable. In the present paper we consider the stably stratified Ekman boundary layers (henceforth referred to as SBLs), i.e., the boundary layers affected by the stable static stability and the Earth rotation. Moreover we focus on regular SBLs adjacent to the surface, in which the velocity shear is strong enough to maintain continuous turbulence holding out against negative buoyancy forces. The SBL depth is then specified as the turbulent layer depth. The "very stable boundary layers" (Mahrt, 1998), characterised by intermittent turbulence concentrated in thin disconnected sub-layers – "pancake structures" and often affected by elevated shears, are not considered.

Although theoretical analysis is given in terms of the atmospheric SBL and experimental data are taken from atmospheric measurements, the proposed SBL depth formulation seems to be basically applicable to the stably stratified upper mixed layers in the ocean or lakes. In the latter layers, two specifically ocean/lake mixing mechanisms should generally be taken into consideration, namely, the Langmuir circulation and the surface wave breaking (see Kantha and Clayson, 2000).

An inherent feature of the SBLs is that they cannot grow infinitely. Indeed, in stable stratification the production of the turbulent kinetic energy is due to the velocity shear, and it is limited to $\int_0^h (\tau \cdot \partial \mathbf{u} / \partial z) dz \sim \overline{U} u_*^2$. Here, $z$ is the height over the surface, $h$ is the SBL depth, $\mathbf{u} = (u,v)$ is the wind velocity, $\tau = \left( \tau_x, \tau_y \right)$ is the vertical flux of momentum, $\overline{U}$ is the SBL mean wind velocity, and $u_*$ is the friction velocity ($u_*^2 \equiv |\tau|_{z=0}$). At the same time the buoyancy flux, $C_{uN}$, in the SBL is a decreasing function of height. Given $F_b = F_{bs} \left( 1 - z/h \right)^m$, $m > 0$, the energy loss through overcoming the negative buoyancy forces becomes $\int_0^h F_b dz \sim F_{bs} h / (1+m)$, i.e., it increases with increasing depth of the layer. Here, $F_b = \beta F_\theta + 0.61 g F_q$, $F_\theta$ and $u_*$ are the fluxes of potential temperature, $\theta$, and specific humidity, $q$, respectively, $g$ is the acceleration due to gravity, $\beta = g/T_0$ is the buoyancy parameter, $T_0$ is a reference value of the absolute temperature, and the subscript "s" is used to mark the near-surface values. Comparing the energy production and the energy loss immediately puts an upper limit on the equilibrium depth of the SBL,

$$h < (1+m)(\overline{U}/u_*)L \sim 10^2 L.$$  (1)

Here, $u_*/\overline{U}$ is the drag coefficient (a variable parameter with typical value ~0.02 in stable stratification), and

$$L \equiv -u_*^3 / F_{bs}$$  (2)

is the Monin-Obukhov length scale.

Alternatively a restriction on the SBL depth is deduced by considering of the bulk Richardson number,

$$\mathrm{Ri}_{SBL} = h \Delta b / \overline{U}^2,$$  (3)

where $\Delta b$ is the increment in buoyancy, $b = \beta\theta + 0.61q$, across the layer. The equilibrium SBL depth is estimated diagnostically from measured or modelled vertical profiles of the wind velocity and buoyancy, $u(z)$ and $b(z)$, assuming that the SBL evolves until $\mathrm{Ri}_{SBL}$ reaches a standard critical value (e.g., Troen and Mahrt, 1986). Taking the conventional value of $\mathrm{Ri}_{SBL} \sim 1$ and the above typical value of $u_*/\overline{U}$ ~0.02, Eq. (3) imposes an upper limit on of the SBL depth,

$$h < \sqrt{\mathrm{Ri}_{SBL}}\, \frac{\overline{U}}{u_*}\, \frac{u_*}{N} \sim 50 \frac{u_*}{N}\,, \tag{4}$$

where $N \equiv \sqrt{\Delta b / h}$ is the SBL mean Brunt-Väisälä frequency.

The above analysis suggests that SBLs have a tendency to evolve towards a quasi-steady state characterised by equilibrium SBL depths. The inequalities Eq. (1) and Eq. (4) are derived regardless concrete features of the SBL dynamics. The dimensionless coefficients on their right hand sides are by no means constant. They depend on the full set of the SBL governing parameters including the friction velocity, $u_*$, the near-surface buoyancy flux, $F_{bs}$, the Coriolis parameter, $f$, and the Brunt-Väisälä frequency, $N$, in the free flow above the SBL[1]. Derbyshire (1990) have given a detailed discussion of the concept of equilibrium or quasi-equilibrium geophysical (rotating) SBLs. As follows from the Galperin et al. (1989) advanced turbulence closure model for oceanic SBLs, the above limits are hardly applicable to non-rotating SBLs.

A number of depth scales were proposed to measure the equilibrium SBL depth, $h_E$ (see, e.g., an overview of the oceanic upper mixed layer models in Zlitinkevich et al., 1979). The basic scales are

(i)     $h_E \propto u_* / |f|$, for the neutrally stratified SBL in a rotating fluid (Rossby and Montgomery, 1935),

(ii)    $h_E \propto L$, for the SBL dominantly affected by the surface buoyancy flux (Kitaigorodskii, 1960),

(iii)   $h_E \propto u_*^2 / |fF_{bs}|^{1/2}$, for the SBL affected by the surface buoyancy flux and rotation (Zilitinkevich, 1972),

(iv)    $h_E \propto u_* / |fN|^{1/2}$, for the SBL affected by the free-flow stability and rotation (Pollard et al., 1973),

(v)     $h_E \propto u_* / N$, for the SBL dominantly affected by the free-flow static stability (Kitaigorodskii and Joffre, 1988).

Having regard to existence of the equilibrium SBL depths, it is conceivable that reasonably slow, gradual variations in the SBL depth should satisfy a relaxation equation

$$\frac{dh}{dt} = w_h - (h - h_E)/t_*\,, \tag{5}$$

where $t_*$ is the relaxation time scale, and $h$ and $h_E$ are the actual and the equilibrium depths of the SBL (e.g., Mahrt, 1981), $w_h$ is the large-scale vertical velocity at the SBL upper boundary, $dh/dt = \partial h/\partial t + u\partial h/\partial x + v\partial h/\partial y$, $u$ and $v$ are the wind velocity components along the $x$ and $y$ axes, respectively.

---

[1] Considering baroclinic SBLs the list of the governing parameters should be extended including the geostrophic-wind shears. The present paper focuses on barotropic SBLs.

For the neutrally stratified Ekman layer, dimensional analysis immediately suggests the expressions $h_E \propto u_* / |f|$ and $t_* \propto |f|^{-1}$ (Khakimov, 1976). For the Ekman layer affected by the earth rotation and the surface buoyancy flux, Mahrt (1981) gave a comprehensive review of early SBL depth models. It is likely that no prediction equation was proposed until present for the Ekman layer affected by the free-flow stability.

Eq. (5) is not applicable to non-steady regimes with very fast deepening of the mixed layer against stably stratified undisturbed flow. Here, the growth of the SBL is often accompanied by discontinuities in the velocity and density profiles and turbulent entrainment at the SBL outer boundary. Then the SBL depth equation becomes $dh / dt = w_h + w_e$, where $w_e$ is the entrainment rate (e.g., Kato and Phillips, 1969; Kraus, 1977; Zilitinkevich et al., 1979). Fast deepening of the oceanic SBL is observed when the wind stress at the water surface suddenly increases, with the result that the upper mixed layer as a whole strongly accelerates relative to the underlying thermocline. However, this sort of development is not typical of atmospheric SBLs. In the present paper it is not considered. This paper focuses on analysis of the equilibrium Ekman layer depth and the relaxation-time scales. A comprehensive overview of modern knowledge about atmospheric SBLs is given recently by Smedman (1991), Mahrt (1998, 1999), Mahrt et al. (1998).

## 2. Ekman-layer scaling

Considering the boundary layer depth, $h$, the key point is the turbulent kinetic energy (TKE) production. In stable stratification it is controlled by the velocity shear. Given the eddy viscosity, $K_M$, the SBL depth scale can be derived from the momentum balance equations. In the steady state Ekman-layer these equations read (e.g., Garratt, 1992)

$$f(v - v_g) + \frac{\partial}{\partial z} K_M \frac{\partial u}{\partial z} = 0, \quad -f(u - u_g) + \frac{\partial}{\partial z} K_M \frac{\partial v}{\partial z} = 0. \tag{6}$$

Here, $u$ and $v$ are the wind velocity components; $u_g$ and $v_g$ are the geostrophic wind components, $u_g \equiv -(\rho f)^{-1} \partial p / \partial y$ and $u_g \equiv (\rho f)^{-1} \partial p / \partial x$ ($\rho$ is the air density and $p$ is the pressure); whereas the components of the vertical flux of momentum along the horizontal $x$- and $y$-axes are given by $\tau_x = K_M \partial u / \partial z$ and $\tau_y = K_M \partial v / \partial z$ ($x$-axis is aligned with the surface stress to make $\tau_y = 0$ at $z = 0$).

The velocity components, $u$ and $v$, satisfy the boundary conditions

$$u = v = 0 \quad \text{at} \quad z = 0; \quad u \to u_g, \quad v \to v_g \quad \text{at} \quad z \to \infty. \tag{7}$$

In the barotropic flow (when $u_g$ and $v_g$ are depth-constant), differentiating Eqs. (6) over $z$ and then multiplying by $K_M$ yields

$$ f\tau_y + K_M \frac{\partial^2 \tau_x}{\partial z^2} = 0, \quad -f\tau_x + K_M \frac{\partial^2 \tau_y}{\partial z^2} = 0, \tag{8} $$

where the momentum flux components, $\tau_x$ and $\tau_y$, satisfy the boundary conditions

$$ \tau_x = u_*^2, \ \tau_y = 0 \ \text{ at } \ z = 0; \quad \tau_x \to 0, \ \tau_y \to 0 \ \text{ at } \ z \to \infty \tag{9} $$

(remember, the $x$-axis is aligned with the surface stress).

At given $K_M$, Eqs. (8)-(9) immediately yields the vertical profiles of $\tau_x$ and $\tau_y$, and eventually, the depth of the Ekman-layer, $h_E$. Moreover, it is evident that $h_E$ is controlled by the portion of the flow where $K_M$ *is the largest*. As a result, analysis of Eqs. (8)-(9) aimed at the derivation of the Ekman-layer depth scale can be done substituting for the eddy viscosity $K_M$ *its maximum value*, $K_M^*$, typical of the Ekman layer interior and independent of height ($K_M^* = $ constant). Then employing the squared friction velocity, $u_*^2$, to measure the momentum flux and the familiar Ekman depth scale, $\sqrt{2K_M^* / f}$, to measure the height, and switching to the dimensionless variables,

$$ \hat{\tau}_x = \tau_x / u_*^2, \ \hat{\tau}_y = \tau_y / u_*^2, \ \hat{z} = z / \sqrt{2K_M^* / f}, \tag{10} $$

Eqs. (8)-(9) become

$$ \hat{\tau}_y + \frac{1}{2}\frac{\partial^2 \hat{\tau}_x}{\partial \hat{z}^2} = 0, \quad -\hat{\tau}_x + \frac{1}{2}\frac{\partial^2 \hat{\tau}_y}{\partial \hat{z}^2} = 0, \tag{11} $$

$$ \hat{\tau}_x = 1, \ \hat{\tau}_y = 0 \ \text{ at } \ \hat{z} = 0; \quad \hat{\tau}_x \to 0, \ \hat{\tau}_y \to 0 \ \text{ at } \ \hat{z} \to \infty. \tag{12} $$

The problem given by Eqs. (11), (12) is completely self-similar, i.e., it does not include any parameters. This immediately suggests that the only depth scale in the problem is

$$ h_* = \sqrt{2K_M^* / f}. \tag{13} $$

Then the equilibrium Ekman-layer depth, $h_E$, is nothing but a standard portion of $h_*$.

Notice that the solution to Eqs. (11), (12), namely, $\hat{\tau}_x = e^{-\hat{z}} \sin \hat{z}$, $\tau_{\hat{y}} = e^{-\hat{z}} \cos \hat{z}$ is neither needed nor used in the present paper. Moreover, the assumption $K_M = $ constant, although well grounded in the derivation of the Ekman-layer depth scale, would become completely non-realistic if one attempts to apply it to the velocity profiles or the resistance law.

6

## 3. SBL depth equations

To determine the eddy viscosity scale, $K_M^*$, it is sufficient to consider the eddy viscosity profile, $K_M(z)$, in the lover portion of the Ekman layer, the surface layer, where $K_M$ is an increasing function of $z$. Here, the momentum flux can be taken depth constant ($|\tau| = u_*^2$). Then $K_M$ is immediately expressed through the velocity gradient,

$$K_M = \frac{u_*^2}{\partial u / \partial z}.$$
(14)

In the upper portion of the Ekman layer, $K_M$ can only decrease.

In neutral stratification, the velocity gradient and the eddy viscosity profiles in the surface layer are $\partial u / \partial z = u_* / kz$ and $K_M = ku_*z$, where $k \approx 0.4$ is the von Karman constant. Hence the Ekman-layer eddy viscosity scale is $K_M^* \propto u_*h_*$. Then Eq. (13) immediately yields the well-known Rossby and Montgomery (1935) formula,

$$h_E^2 = \left( C_R \frac{u_*}{f} \right)^2,$$
(15)

where $C_R$ is a dimensionless constant. Field data practically never correspond to thoroughly neutral stratification, which is why they can hardly be used to determine $C_R$. A rough estimate of $C_R \sim 0.5$ was obtained from lab experiments and large-eddy simulations by Zilitinkevich and Mironov (1996).

In stable stratification, two different regimes should be distinguished. The concern of the traditional theory is the nocturnal boundary layer. Its lower portion, the surface layer, is adequately described by the classical Monin-Obukhov similarity theory (e.g., Chapter 4 in Monin and Yaglom, 1971). Here, the velocity gradient is

$$\frac{\partial u}{\partial z} = \frac{u_*}{kz} \left( 1 + C_u \frac{z}{L} \right),$$
(16)

where $L$ is the Monin-Obukhov length, Eq. (2), and $C_u$ is known empirical constant estimated as $C_u \approx 2.1$ (Högström, 1995). Eqs. (14) and (16) suggest that $K_M$ turns to its maximum value in the upper portion of the surface layer, $K_M \rightarrow ku_*L/C_u$, so as the eddy viscosity scale is $K_M^* \propto u_*L$. Then Eq. (13) yields the Zilitinkevich (1972) formula,

$$h_E^2 = \frac{C_S^2 u_* L}{|f|},$$
(17)

where $C_S$ is known empirical constant roughly estimated as $C_S \approx 0.7$ (Figure 4.37 in Caughey, 1982). Nieuwstadt (1984) have given an elegant alternative derivation of this formula employing the concept of a limiting Richardson number in the upper portion of the SBL.

Eq. (17) is well supported by data from measurements in mid-latitudinal nocturnal stably stratified boundary layers. However, at high latitudes, this equation with $C_S \approx 0.7$ strongly overestimates the stable boundary layer depth (Handorf, 1999; King and Turner, 1997). A reasonable explanation of this discrepancy lies in essentially different physical nature of the mid- and the high-latitudinal SBLs.

Traditional concept of local turbulence transport in stable stratification, underlying both the MO theory and Eq. (17), is adequate when applied to nocturnal boundary layers separated from the stably stratified free atmosphere by the so-called residual layer. During the first hours of the night, the latter keeps neutral stratification as a memory of the daytime mixing, which prevents interactions between the boundary layer and the free atmosphere through gravity waves.

Clearly, no residual layers are observed on top of long-lived SBLs typical of high latitudes (Forrer and Rotach, 1997; King and Turner, 1997). Here, the stable stratification is observed throughout the troposphere, which is why the vertical wave propagation is not blocked. As a result the SBL turbulence becomes essentially non-local, and the traditional theories fail. Zilitinkevich and Calanca (2000) and Zilitinkevich (2001) have extended the surface-layer similarity theory taking into account possible distant interactions in the thoroughly stable stratification. They provided physical reasoning and experimental data in support of an advanced velocity gradient formulation,

$$\frac{du}{dz} = \frac{u_*}{kz}\left[1 + C_u \frac{z}{L}\left(1 + C_{uN}\mathrm{Fi}\right)\right],$$ (18)

where Fi is the inverse Froude number[2],

$$\mathrm{Fi} = \frac{LN}{u_*},$$ (19)

$C_u$ is known empirical constant ($C_u = 2.1$, after Högström, 1995), and $C_{uN}$ is a new constant introduced in the above papers and determined quite uncertainly ($0.1 < C_{uN} < 0.4$).

---

[2] This parameter (designated by $S$ in Zilitinkevich and Calanca, 2000) quantifies the effect of the free-flow stability on the surface layer turbulence.

Eqs. (14) and (18) give $K_M \to k u_* L / C_u (1 + C_{uN} \mathrm{Fi})$. Then the eddy viscosity scale is $K_M^* \propto u_* L / (1 + C_{uN} \mathrm{Fi})$, and the Ekman layer depth, $h_E$, becomes

$$h_E^2 = \frac{C_S^2 u_* L}{|f|(1 + C_{uN} \mathrm{Fi})}. \tag{20}$$

When $\mathrm{Fi} \to 0$ it reduces to Eq. (17).

Interpolating between the reciprocals of Eqs. (15) and (20) yields

$$h_E = \frac{C_R u_*}{|f|} \left[ 1 + \frac{C_R^2 u_* (1 + C_{uN} \mathrm{Fi})}{C_S^2 |f| L} \right]^{-1/2}. \tag{21}$$

Eq. (21) covers the whole range of the static stability regimes from neutral to strongly stable. It reduces to the Rossby-Montgomery Eq. (15) in the thoroughly neutral stratification and to the Zilitinkevich Eq. (17) in the stably stratified mid latitudinal SBLs capped by neutrally stratified residual layers (Fi<<1).

Moreover, when the SBL is dominantly affected by the free-flow stability (Fi>>1), Eq. (21) reduces to the Pollard et al. (1973) formula,

$$h_E = \frac{C_S}{\sqrt{C_{uN}}} \frac{u_*}{\sqrt{|f| N}}. \tag{22}$$

Eq. (22) is widely used in physical oceanography. It describes the regime when the static stability in the thermocline affects the upper mixed layer depth much stronger than the buoyancy flux through the water surface. Oceanographic estimates of the proportionality coefficient designated here by $C_S / \sqrt{C_{uN}}$ fall in the range between 1 to 2 (e.g., Pt. 2 in Kraus, 1977; Zilitinkevich et al., 1979). This gives additional support to the more general Eq. (21). Indeed, meteorological estimates of $C_S = 0.7$ and $C_{uN} = 0.1 \div 0.4$ yield $1 < C_S / \sqrt{C_{uN}} < 2$, in agreement with the above oceanographic estimates.

Estimating the Ekman layer relaxation time, $t_E$, as a time scale of the Brownian-type diffusion of momentum across the layer, yields $t_E \propto h_E^2 / K_M \propto |f|^{-1}$. Then Eq. (5) becomes

$$\frac{dh}{dt} = w_h - C_E |f| (h - h_E), \tag{23}$$

where $C_E$ is an empirical dimensionless constant.

Given empirical constants $C_R$, $C_S$ and $C_{uN}$, Eq. (21) expresses the equilibrium Ekman-layer depth $h_E$ through the familiar Monin-Obukhov scale $L$, Eq. (2) and the dimensionless number Fi, Eq. (19). Then given $C_E$, Eq. (23) allows calculating the actual non-steady Ekman-layer depth, $h$.

## 4. Experimental data

Data sets used in this paper for empirical validation of the proposed SBL depth formulation are taken from three measurement sites (Figure 1), namely,

(i)     Cabauw measurement station (Nieuwstadt, 1984; Van Ulden and Wieringa, 1996),
(ii)    BASIS (Baltic Air-Sea-Ice Study) field experiment  (Launiainen, 1999), and
(iii)   ETH-Greenland expedition in summer 1991 (Ohmura et al., 1992).
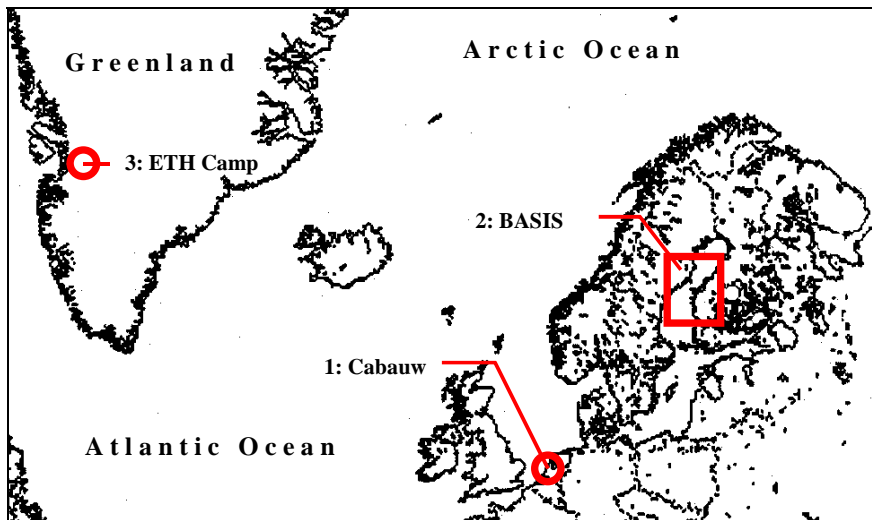


**Figure 1** *Sources of measurements used for empirical validation of the proposed SBL depth formulations: 1 - the Cabauw research measurement station (Nieuwstadt, 1984), 2 - the area of the field experiment BASIS (Launiainen, 1999), 3 - the site of the ETH-Greenland expedition (Ohmura et al., 1992).*

(i) Cabauw
The Cabauw station of the Royal Netherlands Meteorological Institute (KNMI) is located in the western part of the Netherlands (51°58′N, 4°56′E, 2 m.a.s.l.) more than 50 km away from the sea. The 200-meter meteorological mast is surrounded by pastures and meadows, with typical surface roughness length for momentum $z_0 \approx 0.15$ m. The surface elevation changes do not exceed a few metres over 20 kilometres. In the present paper, data from measurements during the period 1977-1979 were used. They included the mean vertical profiles measured at 8 levels between 2 and 200 meters, turbulence measurements, and SODAR measurements. For detailed description of this measurement site and techniques see Vogelezang and Holtslag (1996).

As in the above paper, of the total set of 838 30-minute average turbulence data samples, the cases were selected with negative turbulent fluxes of potential temperature (stable stratification) and the SBL heights less than 180 m (to cover the entire SBL by

the mast measurements and to calculate the Brunt-Väisälä frequency in the free atmosphere above the SBL). As distinguished from Nieuwstadt (1984), the cases with gravity waves were not filtered.

The Monin-Obukhov length, $L$, and the friction velocity, $u_*$, were taken from the turbulence measurements in the surface layer. The SBL height, $h_{SBL}$, was deduced from SODAR measurements through analysis of the backscatter intensity profiles (Nieuwstadt, 1984).

The free-atmosphere Brunt-Väisälä frequency, $N$, was calculated from the temperature gradient in the layer adjacent to the SBL, taken from the mast-based mean profile measurements. Of the selected 196 cases of comparatively shallow SBLs, 65 cases corresponded to well mixed SBLs on the background of pronounced free-flow stability, $N > 0.004$.

High quality measurements at the Cabauw mast allowed quite accurate estimation of the SBL height. Their chief disadvantage is the lack of the mean profiles above 200 meters. The nearest radiosond station, De Bilt, is located 25 km north-east of the Cabauw mast, which is probably too far for the purposes of this paper.
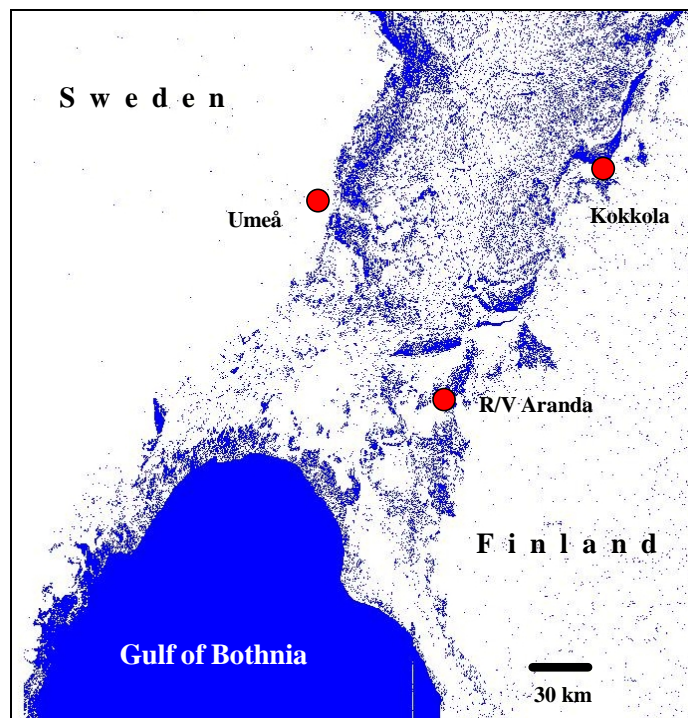


**Figure 2** *Measurement sites, Umeå, Kokkola and R/V Aranda, in the field experiment BASIS, 16 February to 7 March 1998. The Radarsat map (after Launiainen, 1999) shows the border of the ice cover in the Gulf of Bothnia during the experiment.*

(ii) BASIS
The field experiment BASIS (Baltic Air-Sea-Ice Study – Launiainen, 1999) was performed during 16 February – 7 March 1998 at three sites in the Gulf of Bothnia region, namely, Umeå, Kokkola and R/V Aranda (Figure 2). The landscapes around

Umeå and Kokkola represent almost flat snow-covered meadows and low forests (Figure 3). Here, the surface elevations change smoothly and do not exceed a few metres. At larger scale, within 80 and 30 kilometres from the sea on the Finnish and Swedish sides, respectively, they do not exceed one hundred metres. At R/V Aranda, turbulent fluxes of heat, moisture and momentum were measured continuously over the frozen sea. Radio soundings were performed every 6th hour at all three sites.



**Figure 3** *Meteorological 30-m height mast on ice at the Umeå station on the Swedish coast of the Gulf of Bothnia.*

The Umeå station was equipped with a 30 meter tower (Figure 3) erected at the shoreline at Lövöudden (63° 40,5' N, 20° 24,0' E), which is a small peninsula about 25 km south of town Umeå at the Swedish east coast. There was an undisturbed over-ice fetch in the wind direction sectors $50^o$ - $130^o$ and $195^o$ - $250^o$. Wind and temperature profiles were recorded at three heights. Turbulent fluctuations were measured with a Solent sonic anemometer at the 10 m height, and turbulent fluxes were calculated using the eddy-correlation method. The sonic anemometer was re-calibrated in a big wind tunnel and thus corrected for flow distortion prior to being installed on the tower. The calibration procedure is similar to that described by Grelle and Lindroth (1994). The sampling rate was 20 Hz.

The Kokkola station was situated on the sea ice in a bay near Kokkola at the Finnish coast (63° 95' N, 23° 08' E). On a 10x10 m area, four short masts were placed to measure standard parameters and turbulence. Wind speed was measured at 2 m, temperature and radiation, at 1 m. Turbulence was measured at 3.5 m using METEC sonic anemometer. There were at least 3-km open fetches in the sector 135°-315°.

R/V Aranda was anchored in the landfast ice outside the Finnish coast (63° 08,12' N, 21° 14,66' E). A 10-m high mast was erected about 300 m north-west of the ship to measure the temperature and wind profiles (5 levels). Turbulence was measured at 2 m

using METEC sonic anemometer. This station had open ice fetch long enough for all wind directions.

Figure 2 shows the Radarsat map of the Gulf of Bothnia. Here, the open water is black, the land is white and the ice cover is textured (Launiainen, 1999). Referring to this figure, the open water was more than 70 km far from the measurement sites. The cases with winds blowing from open waters were excluded to exclude the convective internal boundary layers.

The data selection was based on the following criteria: (a) stable stratification near the ground ($L > 0$), (b) wind coming from undisturbed wind directions, (c) $h_{SBL}$ clearly detected from the soundings (no internal boundary layers), (d) no front through passing or similar synoptic events.

Altogether 62 cases, including 20 from Kokkola, 25 from R/V Aranda and 17 from Umeå, were selected for further analyses. 48 of these 62 cases exhibited a clearly stable stratification right above the SBL. For the other cases the potential temperature gradient has been set zero. Due to the ice cover, the SBLs over the Gulf of Bothnia occurred during daytime. The soundings from the three stations were put in one data set. Earlier data divisions did not show large differences between the sites (taking winds coming from offshore).

The Monin-Obukhov length, $L$, and the friction velocity, $u_*$, were taken from the surface turbulence measurements. The accuracy of turbulence measurements reduces due to inadequate statistical sampling. According to Dyer et al. (1982), for sampling periods of about one hour, the statistical error in determining the momentum flux is $\pm 15\%$.
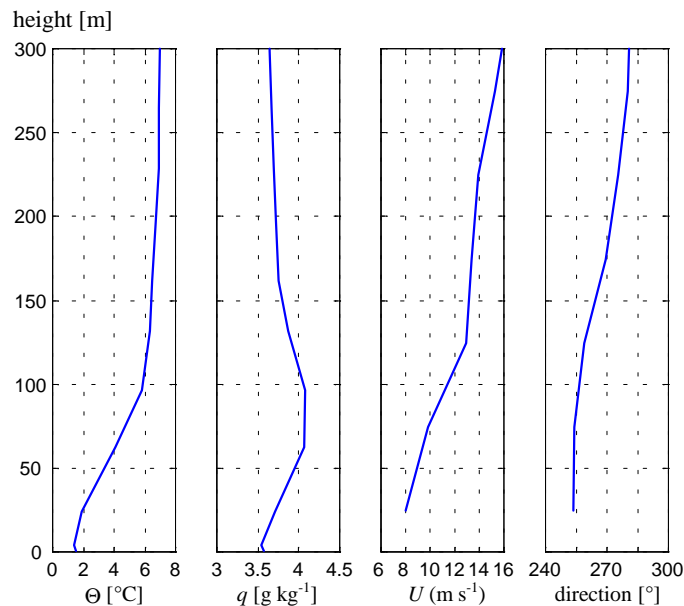


**Figure 4** *Vertical profiles of potential temperature, specific humidity, wind speed and wind direction in a long-lived SBL (Umeå, 20.02.98, 18 UTC).*

The Brunt-Väisälä frequency, $N$, was deduced from the radiosond temperature gradient in the layer adjacent to the SBL. In Figure 4 this is the layer immediately above 100 m. For the surface layer parameters, 30-minute mean values from the launching time of the radiosond plus/minus 15 minutes were chosen.

The SBL height, $h$, was taken from the radiosond profiles by the method of first temperature discontinuity (Hanna, 1969; Wetzel, 1982; Smedman, 1991). In most cases the inversion depth was considered as the proxy for $h_{SBL}$. To avoid or to minimise errors in the determination of $h$ in the thoroughly stable stratification, some cases with unclear temperature discontinuity/fracture were either rejected or reanalysed using the vertical profiles of specific humidity and wind velocity. The BASIS (as well as Cabauw) data were used to verify the diagnostic SBL depth formulation. Accordingly data from measurement in transition times were basically rejected.

(iii) ETH-Greenland
Data from the summer 1991 Swiss Federal Institute of Technology (ETH) Greenland expedition (Ohmura et al., 1992) were used for empirical validation of the prognostic SBL depth formulation. Here, measurements were carried out at the equilibrium line altitude, Paakitsoq (69°34′25″ N, 49°17′44″ W, 1155 m.a.s.l.), western Greenland ice sheet (Figure 1). They included vertical profile measurements on the 30-m meteorological mast, radiation measurements, upper air sounding, turbulence measurements, snow and ice investigations and synoptic observations.

Zilitinkevich and Calanca (2000) have already used (and briefly described) these data in their analysis of the surface-layer scaling for long-lived SBLs.

The mean wind speed and temperature were measured over 30-minute intervals at eight levels on the tower. Three sonic anemometers at 2, 10 and 30 m were used to record the high-frequency fluctuations of the wind speed and temperature. The sampling frequency was 21 s$^{-1}$.

The conditions in the lower troposphere were monitored twice a day with radiosondes. The temperature data were used to specify the height of the inversion layer (typically at some 70 to 200 m above the ground), assumed to be a first order estimate of the PBL height.

Consequently, the Brunt-Väisälä frequency, $N$, was calculated from the potential temperature profiles as a bulk frequency in the layer between the SBL height, $h$, and 500 m above the ground. A time series of $N$ with the same resolution (30 min) as time series for mean gradients and turbulent fluxes was produced from the twice-daily values by linear interpolation in time.

In 1991, stable or neutral stratification within the boundary layer occurred at the expedition site during the summer. The snow was melting so that the surface temperature could not grow higher than 0°C, whereas the air was typically positive. This makes the expedition data set especially convenient for empirical validation of the

prognostic SBL depth formulation. The ETH-Greenland data for 24-25 of July 1991 were chosen, because no residual layer was observed in this period.

## 5. Empirical validation of the proposed SBL depth equations

For empirical validation of the proposed SBL depth equations (Section 3) and estimation of dimensionless constants involved (especially the new constants $C_{uN}$ and $C_E$) the following statistical criteria and parameters are used:
(i)      the bias (the average difference between paired simulations and measurements),
(ii)     the root mean square error (RMSE),
(iii)    the correlation coefficient,
(iv)    the regression coefficient.
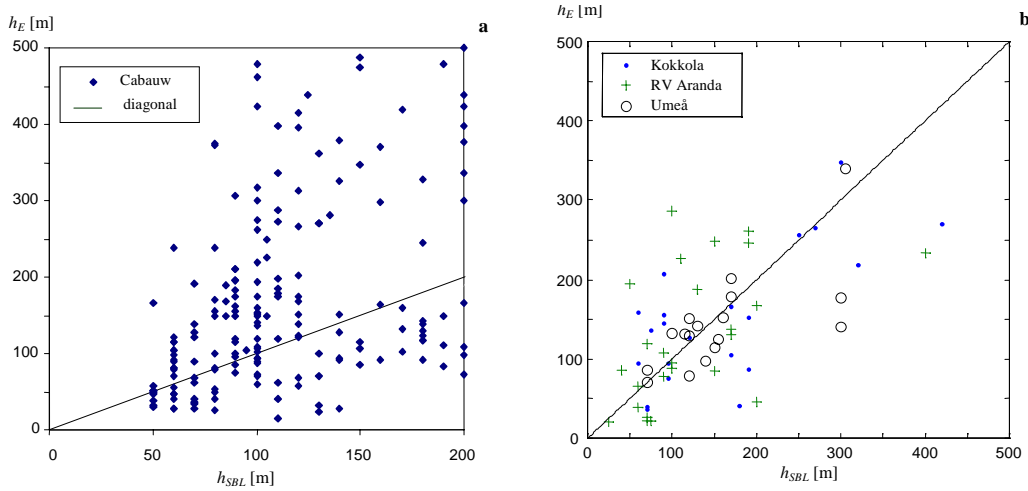


**Figure 5** *Comparison of the measured SBL depths, $h_{SBL}$, with $h_E$ calculated after Eq. (21) using the earlier values of empirical constants $C_R = 0.5$, $C_S = 0.7$ and $C_{uN} = 0.2$ : a) for Cabauw, b) for BASIS.*

Figure 5 shows preliminary comparison of the SBL depths: measured, $h_{SBL}$, and calculated, $h_E$, after Eq. (21) using the earlier estimates of the constants $C_R = 0.5$, $C_S = 0.7$ and $C_{uN} = 0.2$. Figure 5a is a scatter diagram for Cabauw and Figure 5b, for BASIS. Here, a general correspondence is clearly seen, however the spread of data points is quite pronounced. For the BASIS data the correlation coefficient is 0.56, the regression coefficient is 0.94, the bias is 4.2 m and RMSE is 72 m. For the Cabauw data the correlation coefficient is 0.46, the bias is 9.5 m and RMSE is 122 m.

As illustrated in Figure 5a, the scatter increases with increasing SBL heights. Major errors occur at $h_{SBL} \sim 200$ m. This is only natural due to the lack of knowledge about the mean profiles in the vicinity of the SBL top, in particular, poor accuracy in the calculation of the free-flow Brunt-Väisälä frequency. Accordingly, the Cabauw data for $170 < h_{SBL} < 200$ are excluded from the further analysis.

To validate Eq. (21), the Cabauw data on the SBL depth are presented in Figure 6 as a plot
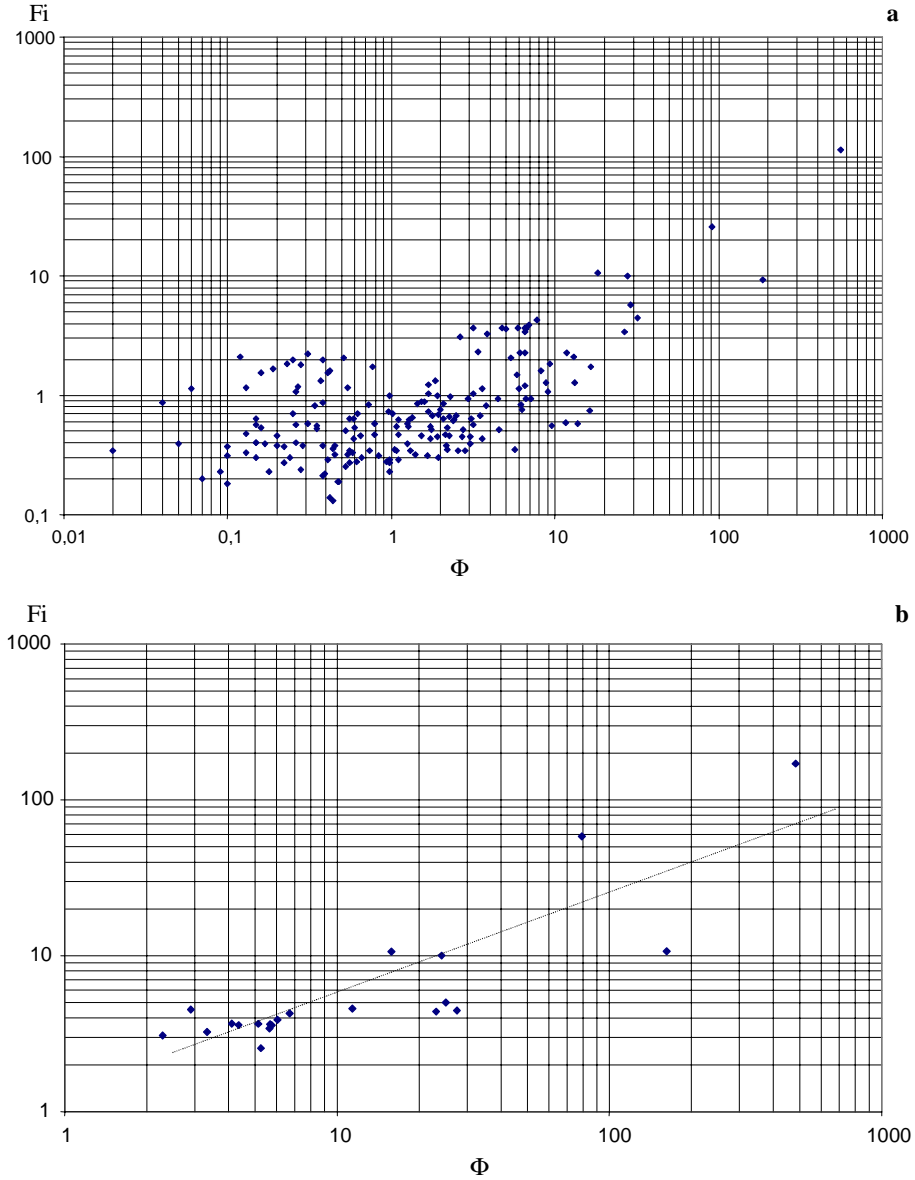


**Figure 6** *Logarithmic-scale plot of the function Φ, Eq. (24), versus the inverse Froude number Fi for Cabauw: a) all data with SBLs, b) data with inversion capped SBLs (Fi>2.5).*

$$\Phi = \left[\left(\frac{C_R u_*}{f h_E}\right)^2 - 1\right]\frac{|f|L}{u_*} \quad \text{versus} \quad \text{Fi} = \frac{NL}{u_*}. \qquad (24)$$

In Figure 6a, quite significant dependence of the function Φ on the inverse Froude number Fi is clearly seen. Here, the correlation coefficient is 0.67. It can be further increased through more careful selection of data. Indeed, the similar dependence for the

cases with strong free-flow stability (Fi > 2.5) presented in Figure 6b exhibits an evidently higher correlation.

In further analysis the dimensionless constants $C_S$ and $C_{uN}$ are estimated using separately the data for near neutral free flows ($Fi \to 0$) and the data for near neutral SBLs ($L \to \infty$). Resolving the neutral-free-flow Eq. (17) for $C_S$, and substituting for $h_E$ the observed SBL depth, $h_{SBL}$, yields

$$C_S = \frac{h_{SBL} \sqrt{|f| u_* / L}}{u_*} \qquad (25)$$

Empirical validation of Eq. (25) against the Cabauw, BASIS and ETH-Greenland data is shown in Figures 7 and 8.
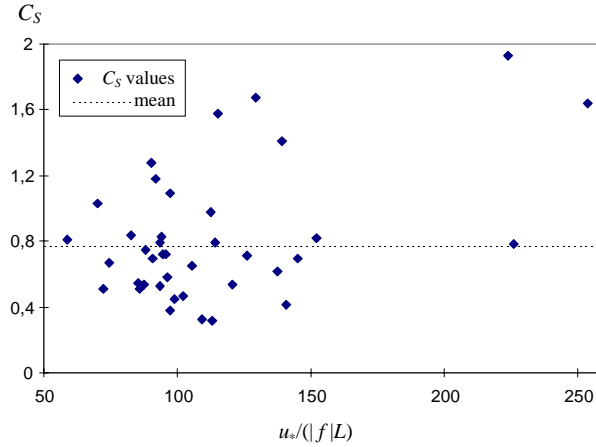


**Figure 7** *Dimensionless coefficient $C_S$, Eq. (25), versus the ratio $u_* / |f| L$ for the near-neutral free-flow regime (nocturnal SBLs), after the Cabauw data with Fi< 0.34.*

In Figure 7 based on the Cabauw data, $C_S$ is presented versus the stratification parameter $u_* / |f| L$. No systematic dependence is seen. $C_S$ varies for from 0.35 to 1.94 with the average value ~ 0.75. The best correlation and minimum bias suggest the optimum value of $C_S = 0.79$.
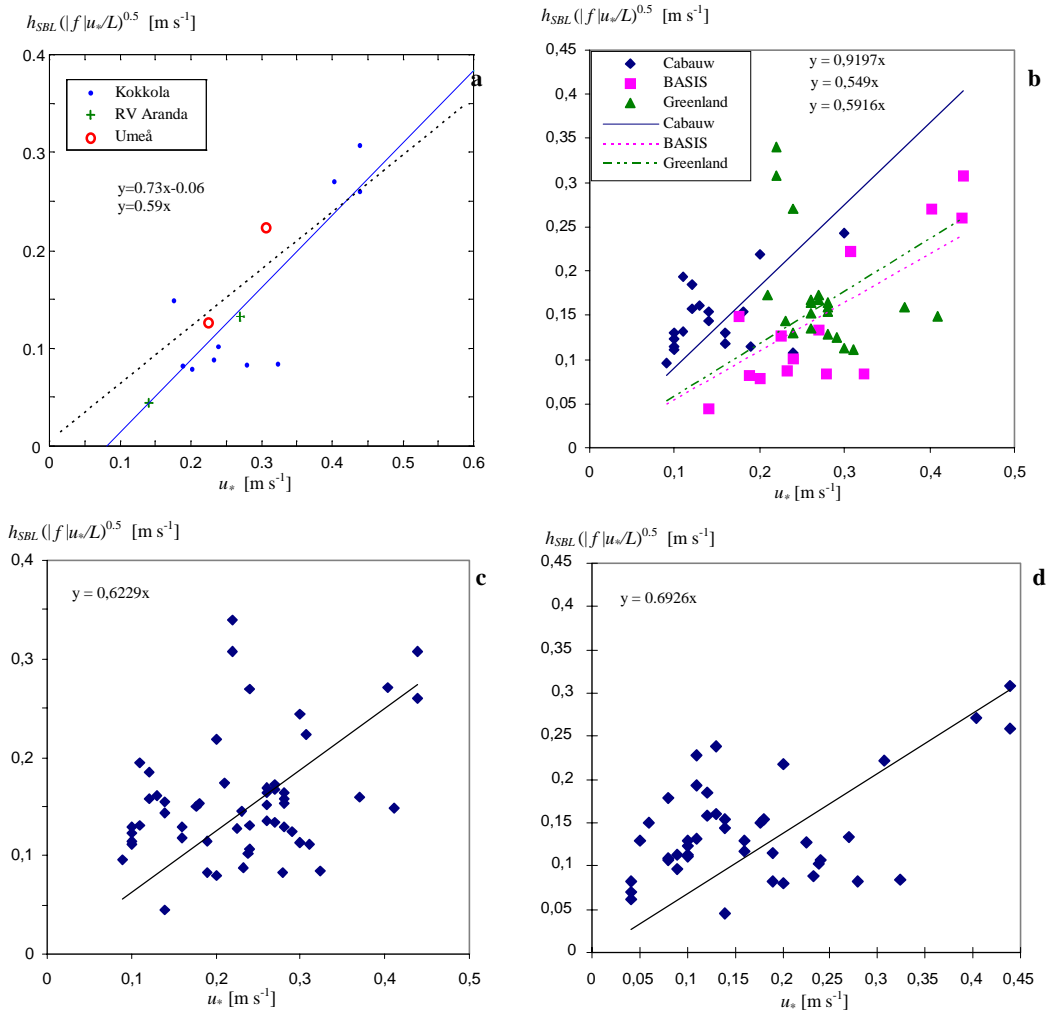
**Figure 8** *Re-estimation of the constant $C_S$ from linear regression for the neutral-free-flow regime (nocturnal SBLs), after the BASIS, Cabauw and ETH-Greenland data: a) BASIS, b) the three data sets, c) joint regression for the 3 data sets, d) joint regression for the Cabauw and BASIS data.*

Figure 8 shows the same analysis employing all three data sets. Here the selection criteria were Fi ≈ 0 and $u_* > 0.11$ m s$^{-1}$ for BASIS and Fi < 0.3 for Cabauw and ETH-Greenland. In Figures 8b and 8c, an additional criterion $u_* > 0.08$ m s$^{-1}$ was applied to the Cabauw data.

Figure 8a represents the three measurement sites of the BASIS experiment. The best-fit linear regression gives the first regression coefficient, the slope ~0.7. However, the second regression coefficient, the intercept, is non zero and gives a shift of the line ~0.08. The forced linear regression with zero intercept gives $C_s = 0.55 \div 0.61$ (Figures 8a and 8b) depending on the selection criteria applied to the BASIS data.

Figure 8b presents the similar estimations of the optimum value of $C_s$ separately from each of the three data sets. As shown in Figure 8b, the Cabauw data give $C_s \approx 0.9$ and

the ETH-Greenland data give $C_s = 0.6$. Fig. 8c suggests the optimum value of $C_s \approx 0.62$ for all data taken together. Of these data, the ETH-Greenland data are probably less applicable to the equilibrium SBL depth problem due to significantly non-steady state and corresponding uncertainties of the interpolation of the SBL depth between the subsequent radio soundings. The most reliable estimate follows from Figure 8d, namely, $C_s = 0.69$ based on the BASIS and the Cabauw data.

In the Earth atmosphere, the near-neutral SBLs (with $L \to \infty$) are practically always capped by a stably stratified free flow, which is why the SBL depth is affected by the free-flow stability. Then the Rossby-Montgomery formula, Eq. (15), is not applicable. Instead, the SBL depth is expressed by a simplified version of Eq. (21) neglecting the first (minor) term in square brackets,

$$h_E = \frac{u_*}{f} \sqrt{\frac{C_S^2 fL}{u_* \left(1 + C_{uN} \mathrm{Fi}\right)}} \ . \tag{26}$$

Here, the square root (a variable coefficient) appears on the r.h.s instead of the constant $C_R$ in Eq. (15). Resolving Eq. (26) for $C_{uN}$ and substituting the observed SBL depth, $h_{SBL}$, for $h_E$ yields

$$C_{uN} = \frac{C_S^2 u_* L - h_{SBL}^2 \, |f|}{h_{SBL}^2 \, |f| \, \mathrm{Fi}} \ . \tag{27}$$

Processing appropriately selected data from Cabauw (namely, those satisfying the conditions $L > 250$ m and Fi > 4), Eq. (27) yields $0.04 < C_{uN} < 0.9$. As shown in Figure 9 a reasonably good correlation is observed in the range $0.25 < C_{uN} < 0.45$ with the best correlation at $C_{uN} \approx 0.35$.
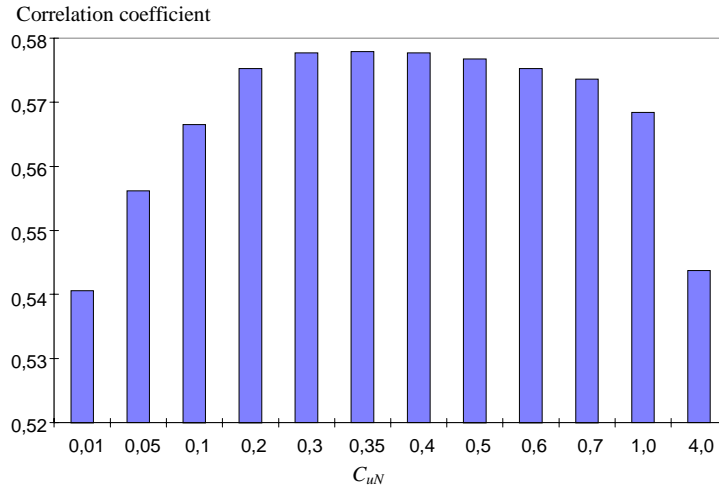
**Figure 9** *Correlation coefficients for different empirical estimates of the coefficient $C_{uN}$ in Eq. (21), after the Cabauw data).*

The similar regression analysis applied to data from BASIS selected to satisfy the condition Fi>5 yields $0.04 < C_{uN} < 0.4$ with the recommended value of $C_{uN} \approx 0.1$. In Figure 10, the SBL heights, $h_E$, calculated after Eq. (26) taking $C_S = 0.74$ and $C_{uN} = 0.1$ are compared with the BASIS empirical estimates of this height, $h_{SBL}$. This figure shows quite good agreement between $h_E$ and $h_{SBL}$, with the correlation coefficient 0.92 and the regression coefficient 0.75. However, the number of data points in this figure is too small for reliable conclusions.
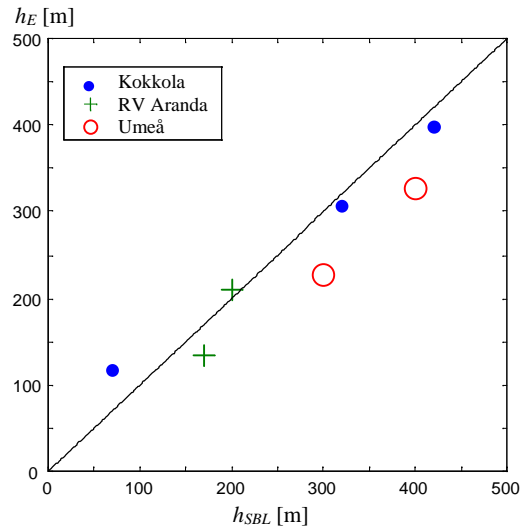


**Figure 10** *Comparison of the measured SBL depths, $h_{SBL}$, with $h_E$ calculated after Eq. (26) taking $C_S = 0.74$ and $C_{uN} = 0.1$, for BASIS.*

Recall that the Greenland data suggest the estimate $C_{uN} \approx 0.2$ (cf. Zilitinkevich and Calanca, 2000), which lies just between $C_{uN} \approx 0.35$ (Cabauw) and $C_{uN} \approx 0.1$ (BASIS).

As already mentioned the thoroughly neutral stratification in the lower atmosphere is practically never observed. Moreover, the general equilibrium SBL depth formulation, Eq. (21), is rather insensitive to the choice of $C_R$. Accordingly, Zilitinkevich and Mironov (1996) deduced an empirical value of $C_R = 0.5$ from large-eddy-simulation (LES) and lab-experiment data. In the present paper an attempt is made to re-evaluate this constant using atmospheric data.
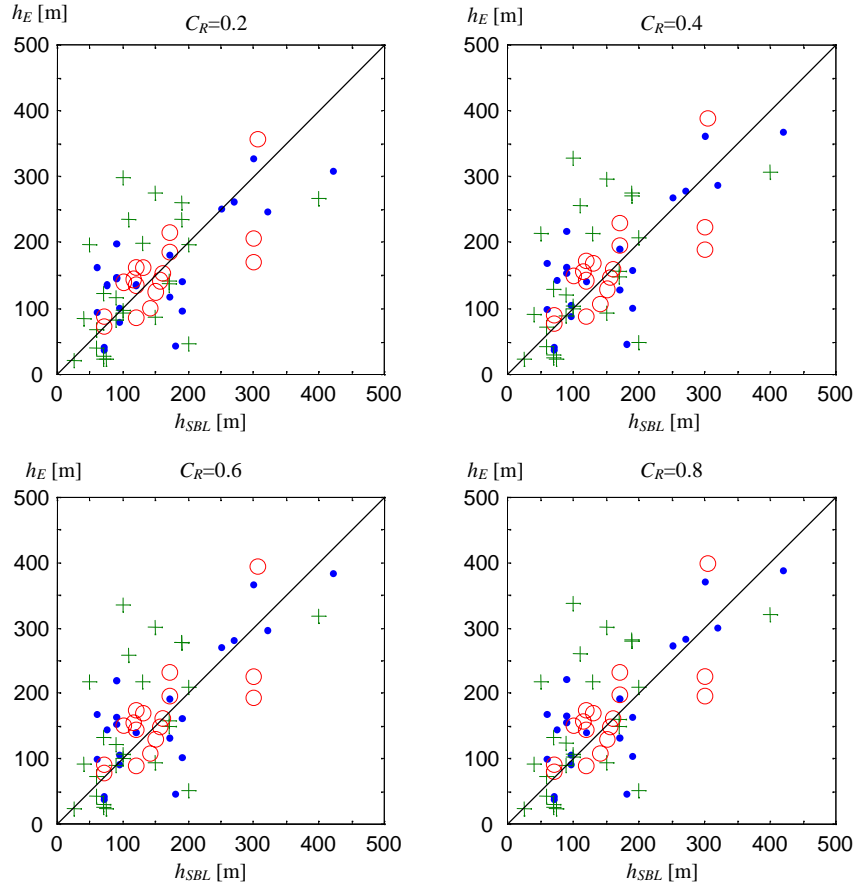


**Figure 11** *Comparison of the measured SBL depths, $h_{SBL}$, with $h_E$ calculated after Eq. (21) taking $C_S = 0.74$, $C_{uN} = 0.1$ and $C_R = 0.2, 0.4, 0.6$ and $0.8$, for BASIS.*

Figure 11 shows comparison of theoretical $h_E$ calculated after Eq. (21) with $C_R$ =02, 04, 0.6 and 0.8 and measured $h_{SBL}$ taken from the BASIS data. Here, the graph with $C_R$ =0.4 exhibits a slightly better correlation than the three others. The similar analysis based on the Cabauw data yields $C_R$ =0.35. The same estimate, $C_R$ =0.35, is recommended recently by Zilitinkevich and Baklanov (2001).

The estimates of $C_R$ from the BASIS data are presented in Table 1. Here, the bias and the RMSE reduce and the regression coefficient increases when $C_R$ decreases from 0.8 to 0.2. At the same time the correlation coefficient decreases when $C_R$ goes below 0.4 and changes insignificantly when $C_R$ falls within the range $0.4 < C_R < 1.0$. Considering all the above uncertainties and a low sensitivity of Eq. (21) to the choice of $C_R$, its tentatively recommended value is $C_R = 0.4$.

Table 1. Bias, RMSE, regression and correlation coefficients for various $C_R$ (taking $C_S = 0.74$ and $C_{uN} = 0.1$)

| $C_R$ | Regression coefficient | Correlation coefficient | Bias (m) | RMSE (m) |
|---|---|---|---|---|
| 0.2 | 0.92 | 0.67 | 2.49 | 68.79 |
| 0.4 | 0.85 | 0.69 | 14.32 | 71.73 |
| 0.6 | 0.83 | 0.70 | 16.94 | 72.81 |
| 0.8 | 0.83 | 0.70 | 17.89 | 73.25 |
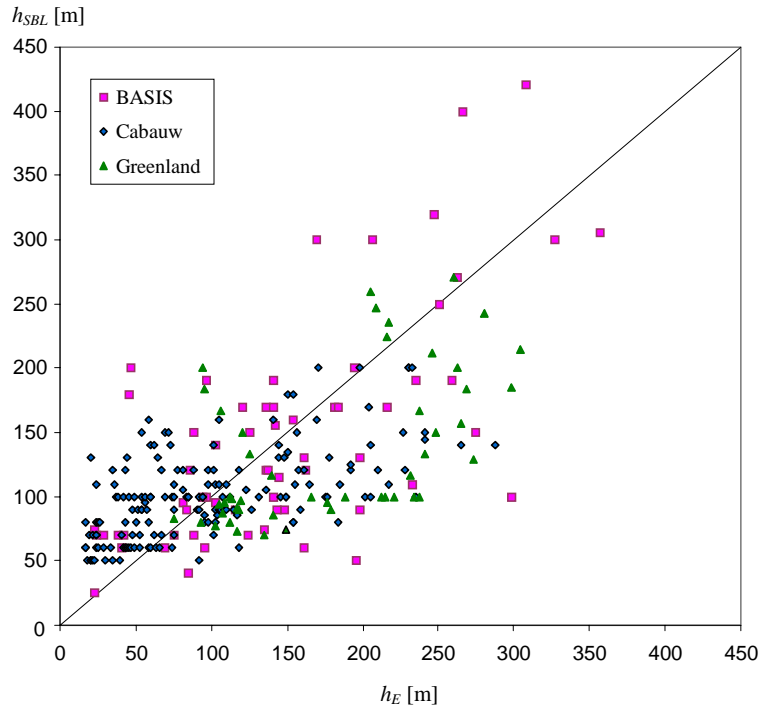


**Figure 12** *Comparison of the measured SBL depths, $h_{SBL}$, with $h_E$ calculated after Eq. (21) taking refined values of the constants $C_R = 0.4$, $C_S = 0.74$ and $C_{u2} = 0.25$, for all data from BASIS, Cabauw and ETH-Greenland.*

Figure 12 shows comparisons of the measured and calculated SBL heights for different data sets: $h_{SBL}$ is taken from measurements and $h_E$ is calculated after Eq. (21) using refined constants, $C_R = 0.4$, $C_S = 0.74$ and $C_{uN} = 0.25$. The correlation coefficients are

0.669 for BASIS, 0.601 for Cabauw, and 0.547 for ETH-Greenland. Compared to Figure 5 (based on the earlier estimates, $C_R = 0.5$, $C_S = 0.7$ and $C_{uN} = 0.2$) Figure 12 shows evidently better performance. For the Cabauw data, the correlation coefficient becomes 0.60 (compared to 0.46), the bias becomes 6.21 m (compared to 9.53 m) and the RMSE becomes 50.89 m (compared to 122.35 m). For the BASIS data, the correlation coefficient becomes $r = 0.62$ (compared to 0.56) and the RMSE becomes 68.78 m (compared to 72.71 m). For the Greenland data, the RMSE becomes 75.01 m. Admittedly, on the background of the observed spread of data, the same comparison employing the earlier estimate of $C_{uN} = 0.2$ based on the surface-layer data (Zilitinkevich and Calanca, 2000) is only slightly worse.

Considerable spread of data in Figures 10-12 is quite understandable. Indeed, half-an-hour averages during non-steady situations might lead to under- or overestimation of the friction velocity or the sensible heat flux, which inevitably results in strong uncertainty of the calculations. For the BASIS and the ETH-Greenland data, the SBL heights are deduced rather uncertainly for the radiosond profiles. For the Cabauw data, when the SBL heights are close to the top of the mast, the calculation of the free-flow Brunt-Väisälä frequency, $N$, becomes very uncertain.
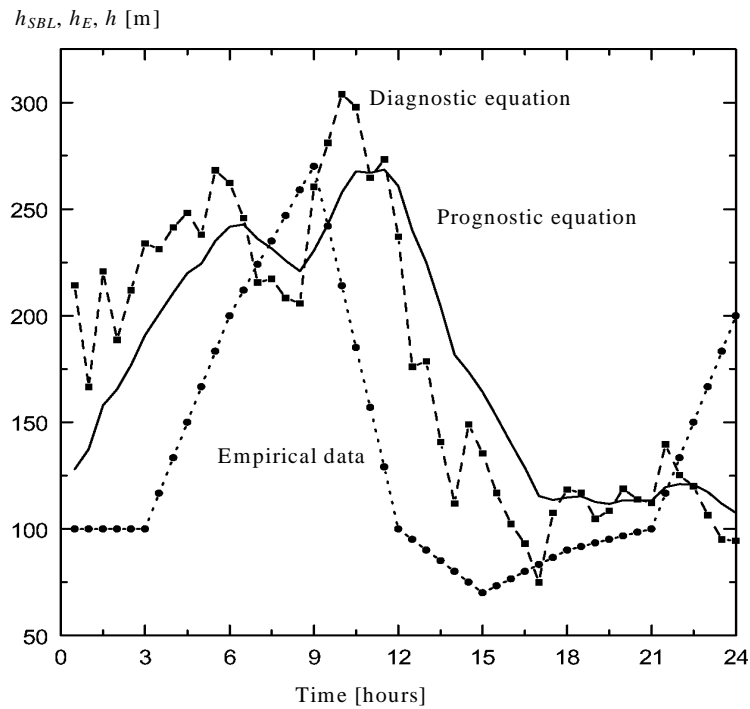


**Figure 13** *Temporal variation of the measured and calculated SBL depths: $h_{SBL}$ – after the ETH-Greenland data (25 July 1991); $h_E$ – after the diagnostic Eq. (21); and h – after the prognostic Eq. (23), taking $C_R = 0.5$, $C_S = 0.74$, $C_{uN} = 0.2$ and $C_E = 1$.*

The prognostic SBL depth equation, Eq. (23), was verified against data from the summer 1991 ETH-Greenland expedition (Ohmura et al., 1992). Here, the height of the inversion layer deduced from the mean temperature profile was identified with the

observed SBL height, $h_{SBL}$. Typically $h_{SBL}$ lied between 70 and 270 m. Figure 13 shows comparison of the three estimates of the SBL height,

(i)     $h_{SBL}$ deduced from the above ETH-Greenland data,

(ii)    $h_E$ calculated diagnostically after Eq. (21) with $C_R = 0.4$, $C_S = 0.74$ and $C_{uN} = 0.2$,

(iii)   $h$ calculated after prognostic equation, Eq. (23), with $C_E = 1$.

The latter value of the relaxation-time constant $C_E$ was obtained from best fitting of the prognostic-equation curve for experimental data. It is worth noticing that the correspondence between the measured and calculated SBL height markedly worsened using $C_{uN} = 0.1$.

Summing up, empirical estimates of the dimensionless coefficients in Eqs. (21) and (23) are $C_R = 0.3 \div 0.5$, $C_S = 0.6 \div 0.79$, $C_{uN} = 0.1 \div 0.35$ and $C_E = 1$. The values recommended for practical applications are $C_R = 0.4$, $C_S = 0.74$, $C_{uN} = 0.25$, and $C_E = 1$.

## 6. Concluding remarks

The proposed formulation for the depth of the barotropic stably stratified Ekman layer (SBL) consists of two operations, first, calculation of the equilibrium SBL depth from the diagnostic Equation (21) and, second, integration of the relaxation-type prognostic Equation (23) to obtain the actual SBL depth.

The diagnostic equation is derived employing the Ekman equations and a recently developed eddy viscosity model accounting for non-local features of long-lived SBLs. In this approach the free-flow Brunt-Väisälä frequency fits naturally into the scheme. This allows linking the meteorological and oceanographic SBL depth formulations.

Scaling analysis given in Section 2 clearly shows that the dependence of the equilibrium Ekman layer depth $h_E$ on the Coriolis parameter $f$ can never be neglected, does not matter how strong is the stratification. Thus from the momentum-balance standpoint any relationships linking $h_E$ to the static stability scales $L$ or $u_*/N$ cannot be immediately applied to the Ekman layer. It is most likely that the SBL in a non-rotating fluid can never achieve an equilibrium state.

Both diagnostic Eq. (21) and prognostic Eq. (23) are validated against atmospheric data. The major factors of the spread of data points in all figures are essential uncertainty of the observed values of the SBL depth and, probably, the mechanisms unaccounted in the background Ekman-layer model (first of all the transition processes and baroclinicity).

Tentatively recommended values of the dimensionless coefficients in Eqs. (21) and (23) are $C_R = 0.4$, $C_{uN} = 0.25$, $C_S = 0.74$ and $C_E = 1$. To refine these coefficients (especially $C_{uN}$) further experimental studies are needed. Here, data from the turbulence and mean-profile measurements in the upper layer of the ocean would be of much use.

**References**

Caughey, S. J., 1982: Observed characteristics of the atmospheric boundary layer. In: *Atmospheric Turbulence and Air Pollution Modelling* (Eds: F.T.M. Nieuwstadt and H. van Dop). D. Reidel, Dordrecht, etc., 107-158.

Derbyshire, S. H., 1990: Nieuwstadt's stable boundary layer revisited. *Quart. J. Roy. Meteor. Soc.*, **116**, 127-158.

Dyer, A. J. et al., 1982: An international turbulence comparison experiment (ITCE 1976). *Boundary-Layer Meteorol.*, **31**, 303-323.

Forrer, J. and Rotach, M. W., 1997: On the turbulence structure in the stable boundary layer over the Greenland ice sheet. *Boundary-Layer Meteorol.*, **85**, 111-136.

Galperin, B., Rosati, A., Kamtha, L. H., and Mellor, G. L., 1989: Modelling rotating stratified turbulent flows with application to oceanic mixed layers. *J. Phys. Oceanogr.*, **19**, 901-916.

Garratt, J. R., 1992: *The Atmospheric Boundary Layer*. Cambridge University Press, 316 pp.

Grelle, A., and Lindroth, A., 1994: Flow distortion by a Solent sonic anemometer: Wind tunnel calibration and its assessment for flux measurements over forest and field. *J. Atmos. Oceanic. Techol.*,**11**, 1529-1542.

Handorf, D., Foken, T., and Kottmeier, C., 1999: The stable atmospheric boundary layer over an Antarctic ice sheet. *Boundary Layer Meteorol.*, **91**: 165-189

Hanna, S. R.: 1969, The thickness of the planetary boundary layer. *Atmosph. Environm.*, **3**, 519-536.

Högström, U., 1995: Review of some basic characteristics of the atmospheric surface layer. *Boundary-Layer Metorol.*, **78**, 215-246

Kantha, L. H., and Clayson, C. A., 2000: *Small Scale Processes in Geophysical Fluid Flows*. Academic Press, San Diego, etc., 883 pp.

Kato, H., and Phillips, O. M., 1969: On the penetration of a turbulent layer into stratified fluid, *J. Fluid. Mech.*, **37**, 643-665.

Khakimov, I. R., 1976: The wind profile in the neutrally stratified atmospheric boundary layer, Izvestiya, *Atmospheric and Oceanic Physics*, **12**, 628-630.

King, J., and Turner, J., 1997: *Antarctic Meteorology and Climatology*. Cambridge University Press.

Kitaigorodskii, S. A., 1960: On the computation of the thickness of the wind-mixing layer in the ocean, Izvestiya, *Ser. Geophys.*, No.3, 425-431.

Kitaigorodskii, S. A., and Joffre, S. M., 1988; In search of simple scaling for the heights of the stratified atmospheric boundary layer, *Tellus*, **40A**, 419-43.

Kraus, E. B., 1977: *Modelling and Prediction of the Upper Layers of the Ocean.* Pergamon Press.

Launiainen, J., (Ed.) 1999: *BASIS-98 Data Report*, International BALTEX Secretariat, Publication No.14, 1999.

Mahrt, L., 1981: Modelling the depth of the stable boundary layer, *Boundary-Layer Meteoriol.*, **21**, 3-19.

Mahrt, L., 1998: Stratified atmospheric boundary layers and breakdown of models. *J. of Theor. and Comp. Fluid Dyn.*, **11**, 263-280.

Mahrt, L., 1999: Stratified atmospheric boundary layers. *Boundary-Layer Meteorol.*, **90**, 375-396.

Mahrt, L., Sun, J., Blumen, W., Delany, T., and Oncley, S., 1998: Nocturnal boundary-layer regimes. *Boundary-Layer Meteorol.*, **88**, 225-278.

Monin, A. S., and Yaglom, A. M., 1971: *Statistical Fluid Mechanics: Mechanics of Turbulence*, The M.I.T. Press, Cambridge, Massachusetts, and London, England, 769 pp.

Nieuwstadt, F. T. M., 1984: The turbulent structure of the stable, nocturnal boundary layer, *J. Atmos. Sci.*, **41**, 2202-2216.

Ohmura, A., Steffen, K., Blatter, H., Greuell, W., Rotach, M., Stober, M., Konzelmann, T., Forrer, J., Abe-Ouchi, A., Steiger, D., and Neiderbäumer, G., 1992: *ETH Greenland Expedition*. Progress Report No. 2, April 1991 to October 1992, Department of Geography, Swiss Federal Institute of Technology, Zürich.

Pollard, R. T., Rhines, P. B., and Thompson, R. O. R. Y., 1973: The deepening of the wind-mixed layer, *Geophys. Fluid Dyn.*, **3**, 381-404.

Rossby, C. G., and Montgomery, R. B., 1935: The layer of frictional influence in wind and ocean currents, *Pap. Phys. Oceanogr. Meteorol.*, **3**, No.3, 1-101. (M.I.T. and Woods Hole Oceanogr. Inst.)

Smedman, A., 1991: Some turbulence characteristics in stable atmospheric boundary layer flow. *J. Atmos. Sci.*, **48**, 856-868.

Troen, I., and Mahrt, L., 1986: A simple model of the atmospheric boundary layer: sensitivity to surface evaporation, *Boundary-Layer Meteorol.*, **37**, 129-148.

Van Ulden, A. P., and Wieringa, J., 1996: Atmospheric boundary layer research at Cabauw, *Boundary-Layer Meteorol.*, **78**, 39-69.

Wentzel, P. J.,: 1982: Toward parameterisation of the stable boundary layer. *J. Appl. Meteorol.*, **21**, 7-13.

Vogelezang, D. H. P., and Holtslag, A. A. M., 1996: Evolution and model impacts of the alternative boundary layer formulations, *Boundary-Layer Meteorol.*, **81**, 245-269.

Zilitinkevich, S. S., 1972: On the determination of the height of the Ekman boundary layer, *Boundary-Layer Meteorol.*, **3**, 141-145.

Zilitinkevich, S., 2001: Third-order transport due to internal waves and non-local turbulence in the stably stratified surface layer. Submitted to *Quart. J. Roy. Meteorol. Soc.*

Zilitinkevich, S. S., and Baklanov, A., 2001: Parameterisation of stably stratified atmospheric boundary layer height in atmospheric models. Submitted to *Boundary-Layer Meteorol.* (available as DMI scientific report).

Zilitinkevich, S., and Calanca, P., 2000: An extended similarity-theory for the stably stratified atmospheric surface layer. *Quart. J. Roy. Meteorol. Soc.*, **126**, 1913-1923.

Zilitinkevich, S. S., Chalikov, D. V., and Resnyansky, Yu. D., 1979: Modeling the oceanic upper layer. *Oceanologica Acta*, **2**, 219-240.

Zilitinkevich, S., and Mironov, D. V., 1996: A multi-limit formulation for the equilibrium depth of a stably stratified boundary layer, *Boundary-Layer Meteorol.*, **81**, 325-351.

# DANISH METEOROLOGICAL INSTITUTE

## Scientific Reports

Scientific reports from the Danish Meteorological Institute cover a variety of geophysical fields, i.e. meteorology (including climatology), oceanography, subjects on air and sea pollution, geomagnetism, solar-terrestrial physics, and physics of the middle and upper atmosphere.

Reports in the series within the last five years:

No. 96-1
**Poul Frich** (co-ordinator), H. Alexandersson, J. Ashcroft, B. Dahlström, G.R. Demarée, A. Drebs, A.F.V. van Engelen, E.J. Førland, I. Hanssen-Bauer, R. Heino, T. Jónsson, K. Jonasson, L. Keegan, P.Ø. Nordli, **T. Schmith**, **P. Steffensen**, H. Tuomenvirta, O.E. Tveito: North Atlantic Climatological Dataset (NACD Version 1) - Final report

No. 96-2
**Georg Kjærgaard Andreasen**: Daily response of high-latitude current systems to solar wind variations: application of robust multiple regression. Methods on Godhavn magnetometer data

No. 96-3
**Jacob Woge Nielsen, Karsten Bolding Kristensen, Lonny Hansen**: Extreme sea level highs: a statistical tide gauge data study

No. 96-4
**Jens Hesselbjerg Christensen, Ole Bøssing Christensen, Philippe Lopez**, Erik van Meijgaard, Michael Botzet: The HIRLAM4 Regional Atmospheric Climate Model

No. 96-5
**Xiang-Yu Huang**: Horizontal diffusion and filtering in a mesoscale numerical weather prediction model

No. 96-6
**Henrik Svensmark and Eigil Friis-Christensen**: Variation of cosmic ray flux and global cloud coverage - a missing link in solar-climate relationships

No. 96-7
**Jens Havskov Sørensen and Christian Ødum Jensen**: A computer system for the management of epidemiological data and prediction of risk and economic consequences during outbreaks of foot-and-mouth disease. CEC AIR Programme. Contract No. AIR3 - CT92-0652

No. 96-8
**Jens Havskov Sørensen**: Quasi-automatic of input for LINCOM and RIMPUFF, and output conversion. CEC AIR Programme. Contract No. AIR3 - CT92-0652

No. 96-9
**Rashpal S. Gill and Hans H. Valeur**:
Evaluation of the radarsat imagery for the operational mapping of sea ice around Greenland

No. 96-10
**Jens Hesselbjerg Christensen**, Bennert Machenhauer, Richard G. Jones, Christoph Schär, Paolo Michele Ruti, Manuel Castro and Guido Visconti: Validation of present-day regional climate simulations over Europe: LAM simulations with observed boundary conditions

No. 96-11
**Niels Larsen, Bjørn Knudsen, Paul Eriksen, Ib Steen Mikkelsen, Signe Bech Andersen and Torben Stockflet Jørgensen**: European Stratospheric Monitoring Stations in the Artic: An European contribution to the Network for Detection of Stratospheric Change (NDSC): CEC Environment Programme Contract EV5V-CT93-0333: DMI contribution to the final report

No. 96-12
**Niels Larsen**: Effects of heterogeneous chemistry on the composition of the stratosphere: CEC Environment Programme Contract EV5V-CT93-0349: DMI contribution to the final report

No. 97-1
**E. Friis Christensen og C. Skøtt:** Contributions from the International Science Team. The Ørsted Mission - a pre-launch compendium

No. 97-2
**Alix Rasmussen, Sissi Kiilsholm, Jens Havskov Sørensen, Ib Steen Mikkelsen:** Analysis of tropospheric ozone measurements in Greenland: Contract No. EV5V-CT93-0318 (DG 12 DTEE): DMI's contribution to CEC Final Report Arctic Trophospheric Ozone Chemistry ARCTOC

No. 97-3
**Peter Thejll:** A search for effects of external events on terrestrial atmospheric pressure: cosmic rays

No. 97-4
**Peter Thejll:** A search for effects of external events on terrestrial atmospheric pressure: sector boundary crossings

No. 97-5
**Knud Lassen:** Twentieth century retreat of sea-ice in the Greenland Sea

No. 98-1
**Niels Woetman Nielsen, Bjarne Amstrup, Jess U. Jørgensen:**
HIRLAM 2.5 parallel tests at DMI: sensitivity to type of schemes for turbulence, moist processes and advection

No. 98-2
**Per Høeg, Georg Bergeton Larsen, Hans-Henrik Benzon, Stig Syndergaard, Mette Dahl Mortensen:** The GPSOS project
Algorithm functional design and analysis of ionosphere, stratosphere and troposphere observations

No. 98-3
**Mette Dahl Mortensen, Per Høeg:**
Satellite atmosphere profiling retrieval in a nonlinear troposphere
Previously entitled: Limitations induced by Multipath

No. 98-4
**Mette Dahl Mortensen, Per Høeg:**
Resolution properties in atmospheric profiling with GPS

No. 98-5
**R.S. Gill and M. K. Rosengren**
Evaluation of the Radarsat imagery for the operational mapping of sea ice around Greenland in 1997

No. 98-6
**R.S. Gill, H.H. Valeur, P. Nielsen and K.Q. Hansen:** Using ERS SAR images in the operational mapping of sea ice in the Greenland waters: final report for ESA-ESRIN's: pilot projekt no. PP2.PP2.DK2 and 2nd announcement of opportunity for the exploitation of ERS data projekt No. AO2..DK 102

No. 98-7
**Per Høeg et al.:** GPS Atmosphere profiling methods and error assessments

No. 98-8
**H. Svensmark, N. Woetmann Nielsen and A.M. Sempreviva:** Large scale soft and hard turbulent states of the atmosphere

No. 98-9
**Philippe Lopez, Eigil Kaas and Annette Guldberg:** The full particle-in-cell advection scheme in spherical geometry

No. 98-10
**H. Svensmark:** Influence of cosmic rays on earth's climate

No. 98-11
**Peter Thejll and Henrik Svensmark:** Notes on the method of normalized multivariate regression

No. 98-12
**K. Lassen:** Extent of sea ice in the Greenland Sea 1877-1997: an extension of DMI Scientific Report 97-5

No. 98-13
**Niels Larsen, Alberto Adriani and Guido Di-Donfrancesco:** Microphysical analysis of polar stratospheric clouds observed by lidar at McMurdo, Antarctica

No.98-14
**Mette Dahl Mortensen:** The back-propagation method for inversion of radio occultation data

No. 98-15
**Xiang-Yu Huang:** Variational analysis using spatial filters

No. 99-1
**Henrik Feddersen:** Project on prediction of climate variations on seasonel to interannual timescales (PROVOST) EU contract ENVA4-CT95-0109: DMI contribution to the final report:Statistical analysis and post-processing of uncoupled PROVOST simulations

No. 99-2
**Wilhelm May:** A time-slice experiment with the ECHAM4 A-GCM at high resolution: the experimental design and the assessment of climate change as compared to a greenhouse gas experiment with ECHAM4/OPYC at low resolution

No. 99-3
**Niels Larsen et al.:** European stratospheric monitoring stations in the Artic II: CEC Environment and Climate Programme Contract ENV4-CT95-0136. DMI Contributions to the project

No. 00-17
**Sattler, Kai; Huang, Xiang-Yu:** Structure function characteristics for 2 meter temperature and relative humidity in different horizontal resolutions

No. 00-18
**Niels Larsen, Ib Steen Mikkelsen, Bjørn M. Knudsen m.fl.:** In-situ analysis of aerosols and gases in the polar stratosphere. A contribution to THESEO. Environment and climate research programme. Contract no. ENV4-CT97-0523. Final report

No. 00-19
**Amstrup, Bjarne:** EUCOS observing system experiments with the DMI HIRLAM optimum interpolation analysis and forecasting system

No. 01-01
**V.O. Papitashvili, L.I. Gromova, V.A. Popov, O. Rasmussen, S. Vennerstrøm:** Northern polar cap magnetic activity index PCN: Effective area, universal time, seasonal, and solar cycle variations
(In Press)

No. 01-02
**M.E. Gorbunov:** Radioholographic methods for processing radio occultation data in multipath regions

No. 01-03
**Niels Woetmann Nielsen, Claus Petersen**: Calculation of wind gusts in DMI-HIRLAM.

No. 01-04
**Vladimir Penenko, Alexander Baklanov**: Methods of sensitivity theory and inverse modeling for estimation of source parameters and risk/vulnerability areas.